Applied Surface Science 273 (2013) 692–701

Contents lists available at SciVerse ScienceDirect

Applied Surface Science

journal homepage: www.elsevier.com/locate/apsusc

Super-mercuryphobic and hydrophobic diamond surfaces with hierarchical structures: Vanishment of the contact angle hysteresis with mercury

Juan V. Escobar[a,*], Cristina Garza[a], Juan Carlos Alonso[b], Rolando Castillo[a]

[a] Instituto de Física, Universidad Nacional Autónoma de México, PO Box 20-364, DF, México, 01000, Mexico
[b] Instituto de Investigaciones en Materiales, Universidad Nacional Autónoma de México, PO Box 70-360, DF, México, 04510, Mexico

ARTICLE INFO

Article history:
Received 22 December 2012
Received in revised form 23 February 2013
Accepted 24 February 2013
Available online 4 March 2013

Keywords:
Contact angle hysteresis
Mercury
Diamond
Adhesion
Wetting
Mercuryphobic
Hydrophobic
Lotus effect

ABSTRACT

Increased roughness is known to enhance the natural wetting properties of surfaces, making them either more hydrophobic or more hydrophilic. In this work we study the wetting properties of water and mercury drops in contact with boron doped diamond films with progressively increased surface roughnesses. We show how thermal oxidation of a microcrystalline film creates pyramids decorated with sub-micron protrusions that turn its naturally mercuryphobic surface into super-mercuryphobic. With this liquid, we observe the vanishment of the contact angle hysteresis that is expected for rough surfaces as the contact angle approaches *180°*, making small drops of mercury roll along out of the surface at an apparent zero tilt-angle. In contrast, the incorporation of nano-globules on the oxidized surface through a silanization process is necessary to increase the hydrophobic properties of the film for which the contact angle with water reaches 138°. The wetting states that dominate in each case are discussed.

1. Introduction

Inspired by Nature's vast arsenal of amazing and functional surfaces [1,2], a variety of techniques has been developed over the years to tailor the adhesive properties of surfaces for diverse applications in fields that range from microfluidics and biosensing, to the oil, paint, textile and automobile industries. Indeed, studying the basic phenomena of adhesion is important for the development of new materials for specific applications, but it is also interesting from the point of view of fundamental surface science [3,4]. Adhesion is also closely related to Tribology [5], a relatively poorly understood but nonetheless important area of Physics.

It is of particular interest to design and fabricate surfaces that do not get wet by a specific liquid substance [6,7]. As a result, one can have hydrophobic surfaces that are used for self-cleaning windshields, solar panels or camera lenses [2], or oleophobic ones that minimize viscous losses during the transport of oil inside ducts [8]. Controlling and even actively switching the wettability of surfaces can be now achieved through a wide variety of means that can involve optical, mechanical, magnetic, chemical, electrical or thermal techniques. A thorough review on the topic can be found in [9].

It is now recognized that in order to achieve super-hydrophobic states, a combination of a naturally hydrophobic material along with a roughened surface is necessary. This is known as the "faquir effect", since the liquid is supported only by a few points of contact of the roughened surface, thus reducing considerably the real area of interaction. A special case is the "lotus effect", named after lotus leafs that have developed binary structures characterized by micron-sized hills decorated with ~50 nm protrusions on their surfaces that make them super-hydrophobic [2]. Actually, the presence of multi-scaled structures is now recognized as an indispensable condition to achieve super-hydrophobic states [10,11].

The adhesive and frictional behavior of other non-conventional liquids can also be greatly affected by surface roughness. For example, the mobility and adhesion of mercury drops on glass rough surfaces has been studied in the past [12], yielding contact angles (CA) as high as 160° and 150° for the advancing and receding contacts respectively. This difference between the advancing and receding contact angle is called the contact angle hysteresis (CAH). Vanishment of the CAH on rough surfaces is tantamount to achieving a state of non-wettability, which should happen as the contact

* Corresponding author. Tel.: +52 55 6225000x2223.
E-mail addresses: escobar@fisica.unam.mx, escobarjuanvalentin@gmail.com (J.V. Escobar), cgarza@fisica.unam.mx (C. Garza), alonso@unam.mx (J.C. Alonso), rolandoc@fisica.unam.mx (R. Castillo).

0169-4332/$ – see front matter © 2013 Elsevier B.V. All rights reserved.
http://dx.doi.org/10.1016/j.apsusc.2013.02.114

angle approaches 180° [3,4,13] due to the existence of pockets of air trapped at the interface (Cassie wetting state [14]). Adhesion is expected to be very low in this case. On the other hand, for rough surfaces that do not trap air (Wenzel wetting state [15]) the CAH is attributed to the presence of pinning points of the contact line on the surface [4,16,17]. The theoretically predicted vanishment of the CAH can only be observed for solid/liquid combinations that present contact angles that are already relatively high on a flat surface (CA > 140°). Liquid mercury is an ideal candidate to this end due to its very high surface tension (485 mN m^{-1}, about 7 times that of water), provided that the surface against which it is placed is not mercuryphilic- an extreme case is gold, which forms an amalgam with mercury. As will be shown in the present work, the contact angle between mercury and a polished boron doped diamond surface meets this criterion (CA > 150°). In contrast, hydrogen terminated diamond is barely hydrophobic (CA ∼ 91°) [18]. Thus, water and mercury reside on opposite sides of the hydrophobic spectrum, which makes a comparison between the wetting properties of both liquids potentially very rich. Also, the high surface tension of mercury makes it a suitable substance to study the connection between adhesion and wetting phenomena, while the fact that it is conducting could be used to quantify the dynamics of the contact line.

Recently, boron doped diamond-based superhydrophobic surfaces have been fabricated that feature sub-micron scales in the form of nano-grass arrays [19] and nano-wires [9,20]. These surfaces have found technological applications in highly sensitive mass spectrometry or in the field of biological cell adhesion. Indeed, both the chemistry and the topography of diamond surfaces can be modified with relative ease, so that they can be progressively roughened and the corresponding effects on the contact angles can be assessed.

In this paper we study the wetting properties of drops of water and mercury in contact with three boron doped diamond surfaces with increasing surface roughness: (1) a polished single crystal, (2) a microcrystalline one, (3) the same microcrystalline one after aggressive thermal oxidation. As a result we have three surfaces that are very similar chemically, but have radically different roughnesses. We also explore the wetting properties of water on a fourth surface obtained by further modifying the oxidized surface with silane nano-globules.

We find that thermal oxidation of the microcrystalline film creates multi-scale features which lower the adhesion with mercury so much, that drops of mercury roll along out of the surface for an apparent zero tilt angle. This high mobility resembles that of water drops due to Leidenfrost's effect [21]. We compare the CAH of mercury drops in contact with the original microcrystalline film and with the oxidized one, confirming the absence of CAH for the later.

2. Materials and methods

2.1. Mercury

Double distilled mercury was first passed through the small orifice on a filter paper, and then dripped three times though a column of 30% nitric acid. The clean mercury was washed with distilled water and dried with filter paper. Using a syringe, small amounts of mercury were sucked out from the inside of the liquid to avoid any oxide that might have been left on the surface. Mercury is a hazardous liquid which can result in serious body damage if proper care is not taken. Therefore, it was handled in small quantities and kept in caped bottles at all times, while experiments were carried out in an uncarpeted and well-ventilated room, and on a smooth surfaced table that allowed collecting any mercury spills that might have occurred. All mercury cleaning and handling was performed inside a fume hood following the appropriate safety considerations [22].

2.2. Diamond single crystal and microcrystalline film

The wetting properties of three surfaces with different roughnesses are studied: the first one is a boron-doped single crystal natural-type diamond with polished (1 0 0) surface and quoted boron doping concentration of 1×10^{19}/cm^3 (Element Six Corporation, NY, USA). The second one is a 7 μm thick boron-doped microcrystalline diamond film deposited on a silicon substrate (SP3 Corporation, USA). The microcrystalline film has a sheet resistance of 63.6 Ω/sq, and a density of 0.1 microcrystals per square micron, with an average area of 10 μm^2 per crystal. We modify the roughness of this film *via* thermal oxidation to yield the third sample.

2.3. Fabrication and topographical characterization of the oxidized surface

In order to modify the roughness of the surface, the microcrystalline diamond film is heated at 850° for 10 min inside a tubular furnace that has its ends open to the atmosphere. This process thermally oxidizes the diamond crystals, and removes layers of diamond as carbon monoxide. The resistance of the oxidized film increases to ∼500Ω/sq.

Fig. 1 displays AC mode atomic force microscope (AFM, JSPM-4210 JEOL, Japan) images showing how after thermal oxidation there is a significant change in the height of the crystals. The overall thickness of the microcrystalline film decreases by about 1.5 microns, which is consistent with the rate of material removal found in experiments with controlled oxygen pressure and temperature for ambient conditions [23]. Scanning electron microscope (SEM, LV-5600, JEOL, Japan) images of individual crystals (Fig. 1e–f) show that the thermal oxidation of the diamond film leads to the formation of Mayan pyramid-like structures whose tops have linear dimensions of 200 nm or less. Further AFM inspection (Fig. 2a), reveals that the original micro-crystals are not flat, but rather are covered with 40 nm-high protrusions. As a result, after thermal oxidation the surface of the pyramids are not smooth, and their tops are decorated with ∼100 nm-high lumps (Fig. 2b).

A direct consequence of the small size of the tips of the pyramids is the large increase of the electrical resistance of the individual tips, which is readily manifested in current *vs.* apparent-area-of-contact tests. The total electrical resistance of the contact between a mercury drop and the oxidized surface can be modeled with a resistor (the sheet resistance R_s) in series with a contact resistance R_c composed of a group of n highly resistive elements R connected in parallel ($R_c = R/n$). The density per unit area ρ of these resistors in parallel is taken as the average number of crystals per μm^2 (Fig. 3). The apparent area of contact of Fig. 3 was estimated to be (πr^2), where r is the radius of the contact between the mercury and the oxidized diamond, as measured from photographic images for drops of different sizes. Using this model we estimate the average electrical contact resistance of the individual tips to be R = 55 MΩ. We note that this is an upper limit, since it is possible that the mercury is in actual contact with only a fraction of the total pyramids underneath the drop, due to the dispersion of the heights distribution (Fig. 1d). In contrast, the equivalent measurement on the microcrystalline film gives a constant current *vs.* apparent area since the resistance of its micron-sized grains is already small enough as to be insensitive to changes in the area of contact of the order of half a millimeter square.

The aspect ratio of the pyramids was also analyzed. To this end, the average height *vs.* cross sectional radius for each one of 172 oxidized crystals from AFM images was fit to a linear relation. 78.5% of these fits gave an R^2-coefficient better than 0.9, thus validating the use of the term *pyramid*. Of this group, the average angle μ between the external walls of the features and the horizontal axis was μ=157.9° + - 4.81°. In other words, the pyramids are

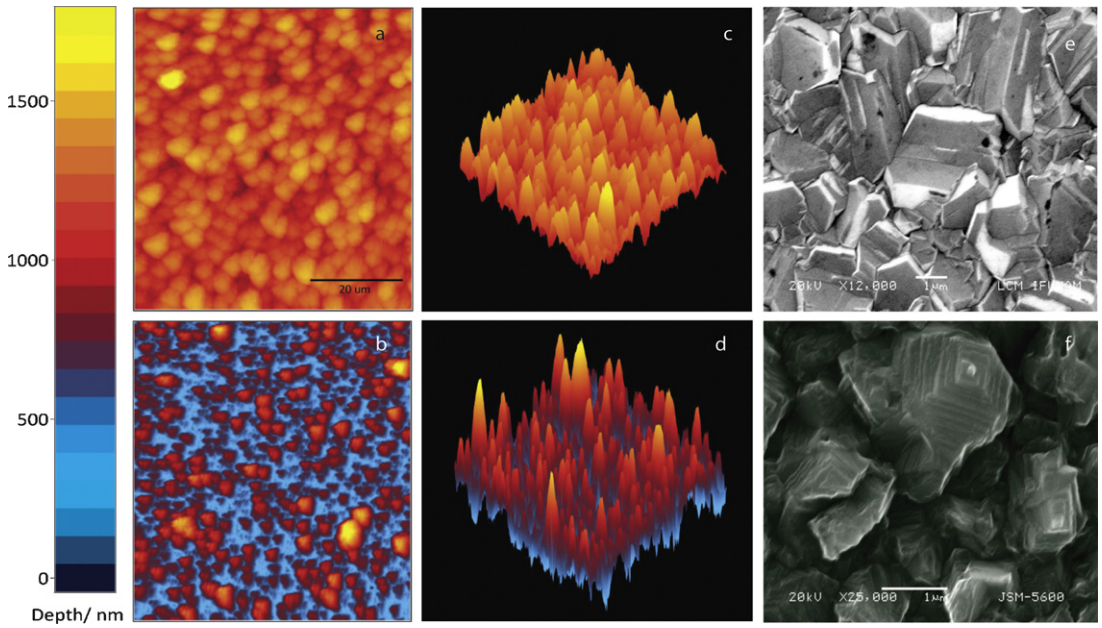

Fig. 1. Effect of thermal oxidation on the topography of the crystals. (a–d) AFM profile of an $60 \times 60\ \mu m^2$ portion of the microcrystalline film (a, c) before and (b–d) after oxidation. The depth of the features increases by about 1.5 μm. (e–f) SEM images of (e) microcrystalline diamond surface, and (f) after thermal oxidation showing the transformation from flat crystals to pyramid-like structures with submicron-size tops.

rather obtuse (aspect ratio = 0.37). The protrusions on their tops form even shallower angles with the horizontal, with typical angles of $\mu = 170^{\circ}$.

Summarizing the topographical characterization, the end result of the thermal oxidation of the microcrystalline film is the creation of a multiple-scaled surface, a necessary condition to fabricate super-solvophobic surfaces.

2.4. Chemical characterization of the surfaces

We characterize the chemical composition of the surfaces with X-ray photoelectron spectroscopy (XPS, VG Microtech ESCA2000 Multilab-UHV system). It is now recognized that the nature and number of oxygen-related chemical groups generated on diamond surfaces depends strongly on the method used for the oxidation

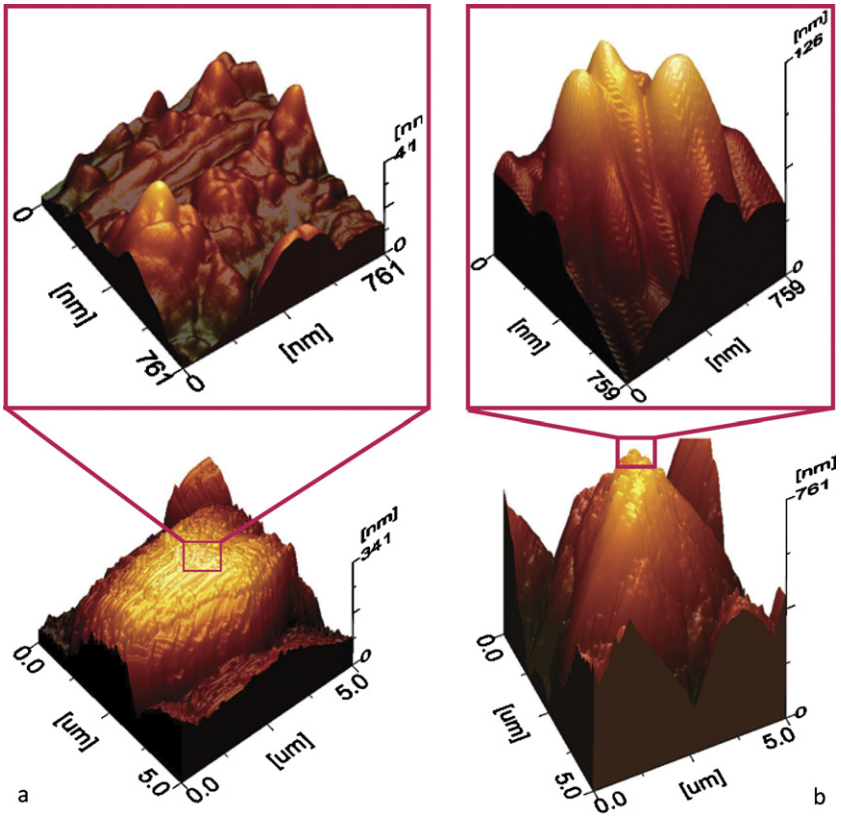

Fig. 2. Presence of sub-micron protrusions on both surfaces. AFM images before (a) and after (b) the oxidation.

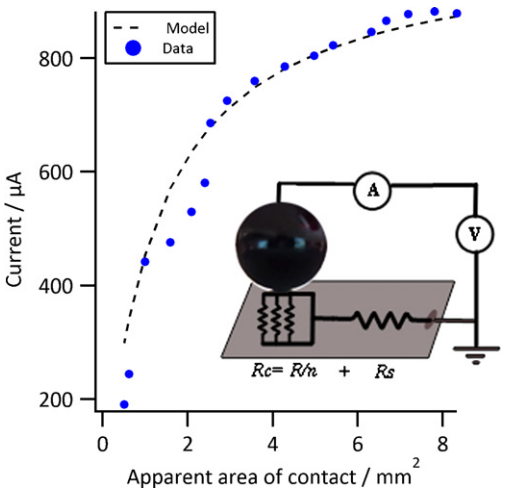

Fig. 3. Current *vs.* apparent area of contact with the oxidized film. Blue dots represent the experimental data, while the dashed line is the calculated current with the model $I = V/(Rs + Rc)$, where $V = 0.5$ V, $Rs = 500\ \Omega$, $Rc = 55\text{M}\Omega/(\text{area} \times \rho)$, and $\rho = (1/10)$ contacts/μm^2 is the density of crystals of the original microcrystalline sample. The apparent area of contact was estimated from photographic images.

process [18,24,25]. Fig. 4 shows the spectrum for the polished surface (Fig. 4a), the as-purchased microcrystalline film (Fig. 4b), the as-oxidized surface (Fig. 4c) and the oxidized surface after baking for 4 h at 200 °C (Fig. 4d). This last thermal treatment was applied to remove as much of the hydroxyl groups as possible, which are typically responsible for drastic changes in the polarizability of the surface [26] that in turn can affect the contact angle [4,18].

After this treatment, the content of single-bonded oxygen is still slightly higher than on the microcrystalline surface and on the single crystal, but already low enough as to make the surface hydrophobic, as will be shown in the results section. Table 1 summarizes the chemical component composition results shown in Fig. 4. The binding energies (BE) used to fit the data are close to those found in the literature for oxidized diamond [18,27].

The BE of the surface defects reported in Table 1 are on the order of 1 eV lower than the main peak at 284.5 eV for sp3 carbon, which suggests that these signals may be related to sp2 carbon [28–30]. In fact, a very similar BE related to the formation of sp2 carbon (283.4 eV) is found during oxygen plasma treatment on polycrystalline boron doper diamond [18]. Another possibility is that the BE's below 284.5 eV correspond to hydrogenated diamond. But in this case the shift in BE is expected to be about 0.5 eV [18,25,31].

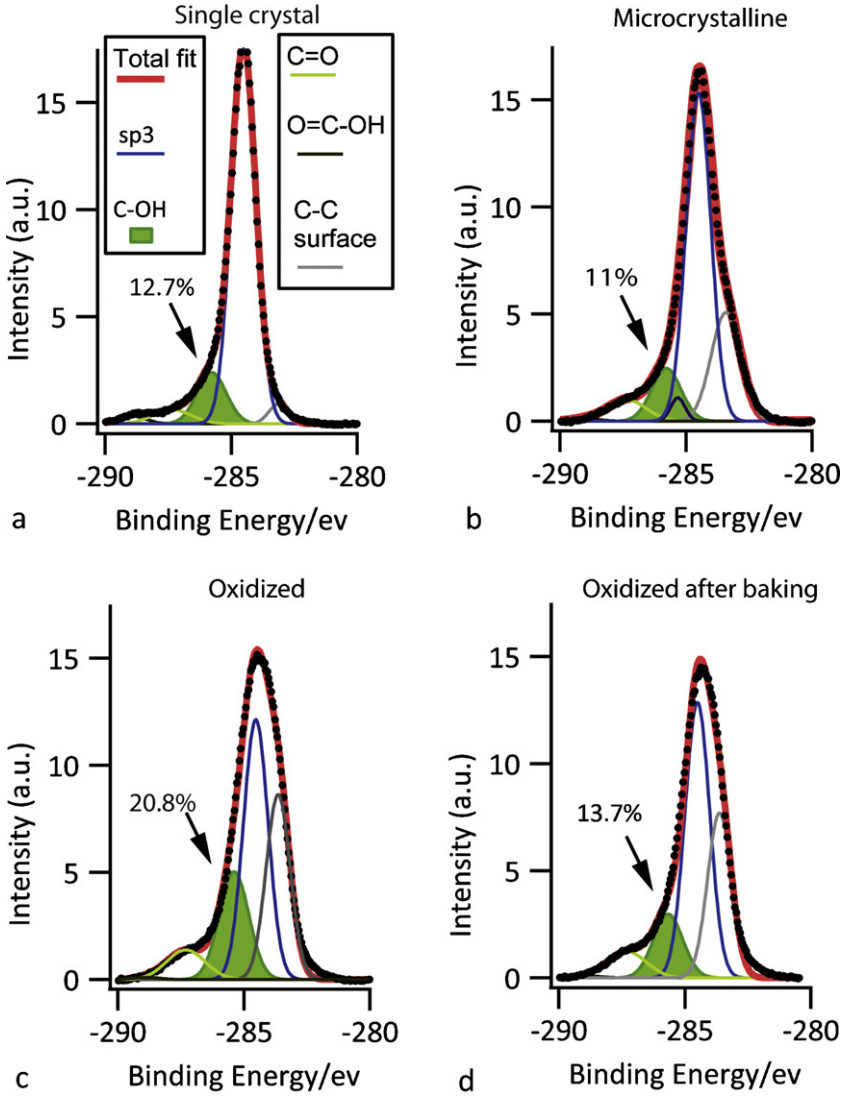

Fig. 4. Chemical characterization of the surfaces. XPS of (a) the single crystal, the (b) microcrystalline diamond film, (c) the microcrystalline film before oxidation and (d) after baking at 200 °C for 4 h.

Table 1
Chemical components and corresponding percentages from XPS.

	Surface defects	sp^3 carbon	Hydroxyl (C—OH)	Carbonyl (C=O)	Carboxyl (O=C—OH)
Binding energy/eV	[a]	284.5	285.78	287.34	288.92
1. Single Crystal	3.1%	77.7%	12.7%	4.6%	1.8%
2. Microcrystalline	22.9%	57.4%	11%	5.8%	0.4%
3. As-oxidized	29.2%	42.1%	20.8%	7.5%	0.4%
4. As-oxidized after 4 h baking at 200°	28.8%	49.6%	13.7	7.5%	0.4%

[a] Surface defects had energies dependent on the specific sample: (1) 283.14, (2) 283.41, (3) 283.64, (4) 283.62 eV. The XPS for the microcrystalline sample has an extra C–N small peak at 285.32 eV which is absent in all others.

We also note that the percentage of oxygen-related components seems high to begin with on both of our non-oxidized samples, as compared to what has been reported in other studies on polycrystalline boron doped diamond [18] and natural type IIb samples [28]. This could be explained by the fact that in the IIb study cited, small amounts of physisorbed water and/or molecular oxygen from air were removed by a cleaning procedure that included mild sputtering, exposure to atomic hydrogen, and annealing at 1000 °C. In contrast, by the nature of the cleaning procedure that we employed, it is possible that our samples were not void of some of these chemical components that may have increased their oxygen content measured with the XPS.

From this analysis, we can assert that the chemical composition of the microcrystalline and the baked oxidized surface are close enough to allow the drastic changes in the wetting properties of these films to be attributed their different surface roughness.

2.5. Silanization process

To create a fourth surface that incorporates an even smaller length-scale, the oxidized diamond film was subject to a silanization process. This process consists of exposing this surface for 1 h to an atmosphere saturated with nitrogen gas that has been bubbled through a pool of diclorodimethylsilane (99%, Sigma Adrich, USA). As a result, the diamond surface is covered with a visible layer of diclorodimethylsilane. The sample is then immersed in chloroform for 42 h to dissolve most of the diclorodimethylsilane, leaving ~35 nm globules attached to the surface. These globules are most likely the product of the polymerization of the the silane compound due to traces of water from ambient vapor. Boron- doped diamond surfaces decorated with "nano-grass" structures and subsequently covered with monolayers of octadecyltrichlorosilane (OTS) or of 1H,1H,2H,2H-perfluorodecyltrichlorosilane (PFTS) with controlled reactions, can result in the formation of superhydrophobic surfaces [19] due to the intrinsic hydrophobicity of both OTS and PFTS. Covering our oxidized diamond films with these substances would probably have a deeper impact on the hydrophobic properties of our films. However, we chose the reaction with diclorodimethylsilane since our goal is to create a forth surface whose hydrophobic properties increase due to the presence of a second length-scale of roughness by the incorporation of nano-globules, and not as a result of an increase of the hydrophobic properties of the substrate itself.

Table 2
Contact angle results.

	Single crystal	Microcrystalline	Oxidized	Nano-patterned
Water	91°	107°	123°	138°
Mercury	155°	162°	>175°	>175°

Fig. 5 shows an SEM image of the oxidized diamond surface after the silanization process.

3. Results

Fig. 6 displays drops of water of ~1.5 mm in diameter resting on the four surfaces (*a* = polished single crystal, *b* = microcrystalline, *c* = oxidized, *d* = oxidized with nano-globules from silanization) showing the effects of surface roughness on the contact angle. On the other hand, the top row of Fig. 7 displays mercury drops in contact with the polished single crystal, the microcrystalline sample,

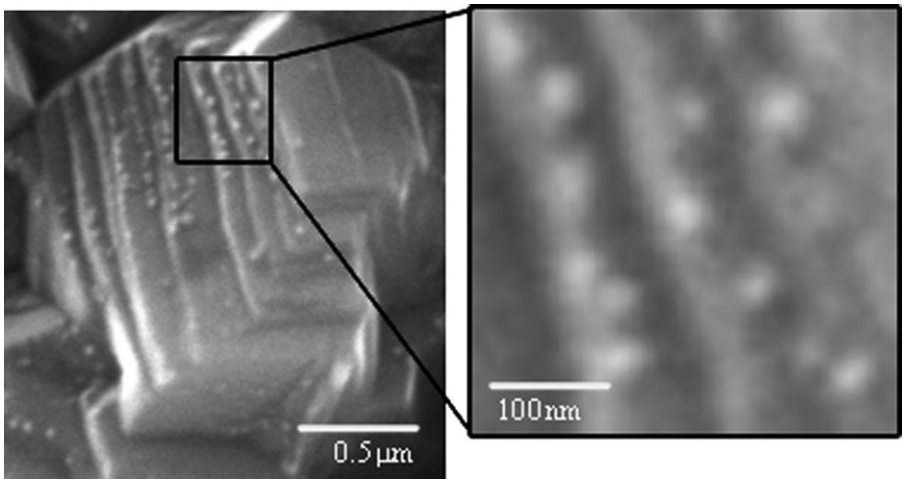

Fig. 5. Oxidized diamond with attached nano-globules. SEM image of the oxidized diamond after the silanization process. The surface is covered with silane nano-globules of about 35 nm in diameter.

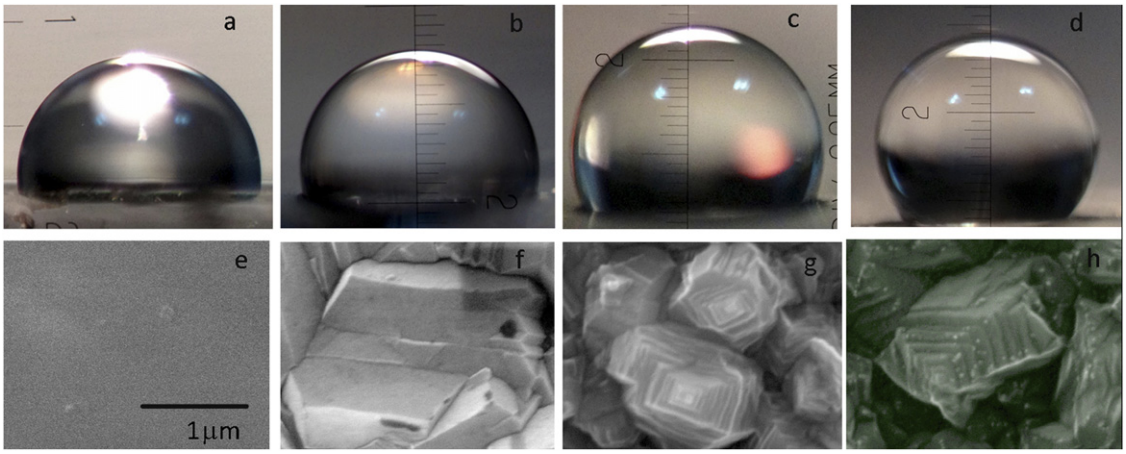

Fig. 6. Contact angle with water. Drops of water in contact with (a) the polished surface, (b) the microcrystalline sample (c) with the oxidized one, and (d) with the oxidized surface with the attached nano-globules. The SEM images underneath each drop show the topography of the corresponding surfaces.

and the oxidized one. Table 2 summarizes the values of the contact angles in each case.

3.1. Water

The contact angle with the single crystal is 91°, which is slightly lower than that found with diamond surfaces fully terminated with hydrogen (CA = 93°) [32] due to the content of oxygen of our sample. The microcrystalline diamond (Fig. 6b) already displays a small improvement on the hydrophobic properties brought about its surface roughness as compared to the singe crystal.

Right after thermal oxidation, the contact angle is zero (not shown) due to the high percentage of C-OH bonds formed during the oxidation process [26,33]. However, after baking at 200° for 4 h the amount of hydroxyl groups decreases (Table 1, Fig. 4d) and the surface is then rendered notably more hydrophobic (Fig. 6c) than before the oxidation (Fig. 6b). Fig. 6d shows the clear effect that the attached nano-globules have on the hydrophobic characteristics of the oxidized film.

3.2. Mercury

In the case of mercury, the contact angle for the single crystal is so high to begin with (Fig. 7a), that progressive roughening of the surface induces a much more pronounced mercuryphobic behavior (Fig. 7b), all the way to a super-mercuryphobic state (Fig. 7c). Actually, adhesion is so miniscule between the oxidized surface and the mercury drop that, regardless of how gently it is placed on it, it was impossible to make a drop stay sessile on the surface since it would quickly roll along out of it. Therefore, a small Teflon ring visible on Fig. 7c was used to prevent the drop's motion.

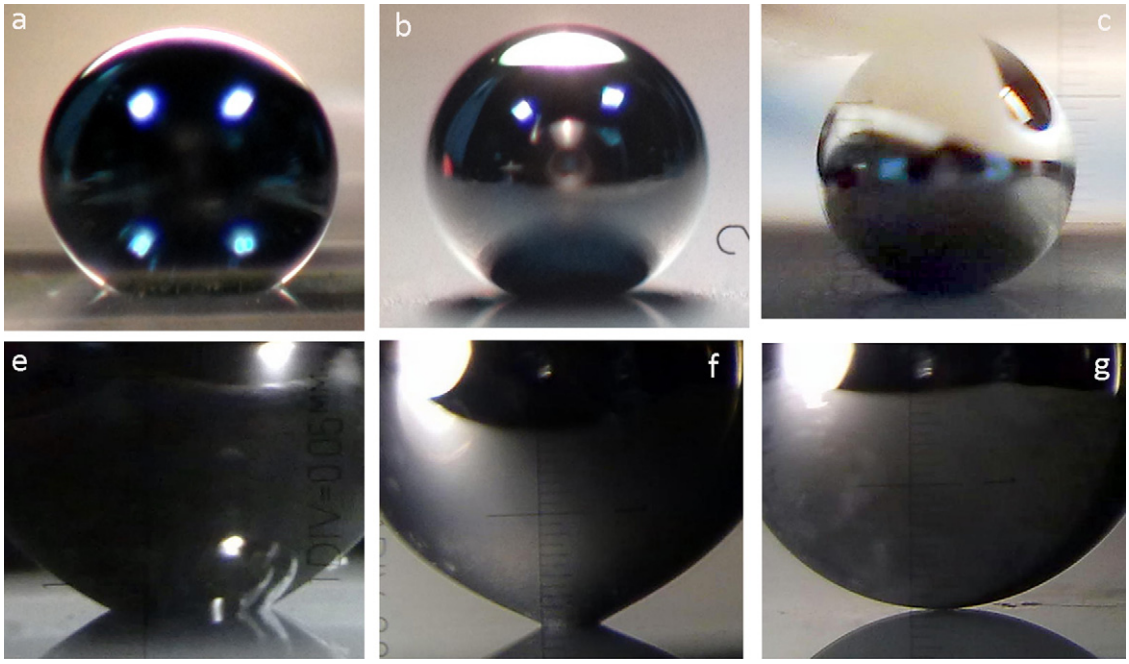

Fig. 7. Contact angle with mercury drops. Contact between drops of mercury resting on the surfaces (top row) and being detached from them (lower row). The columns correspond to (left) the polished singe crystal, (center) the microcrystalline diamond and (right) the oxidized sample. The adhesion between the mercury drop and the oxidized diamond film is so low, that it was necessary to place a Teflon ring (reflected on the drop's surface of Fig. 7c) in contact with the top of the drop to prevent it from rolling out of the film.

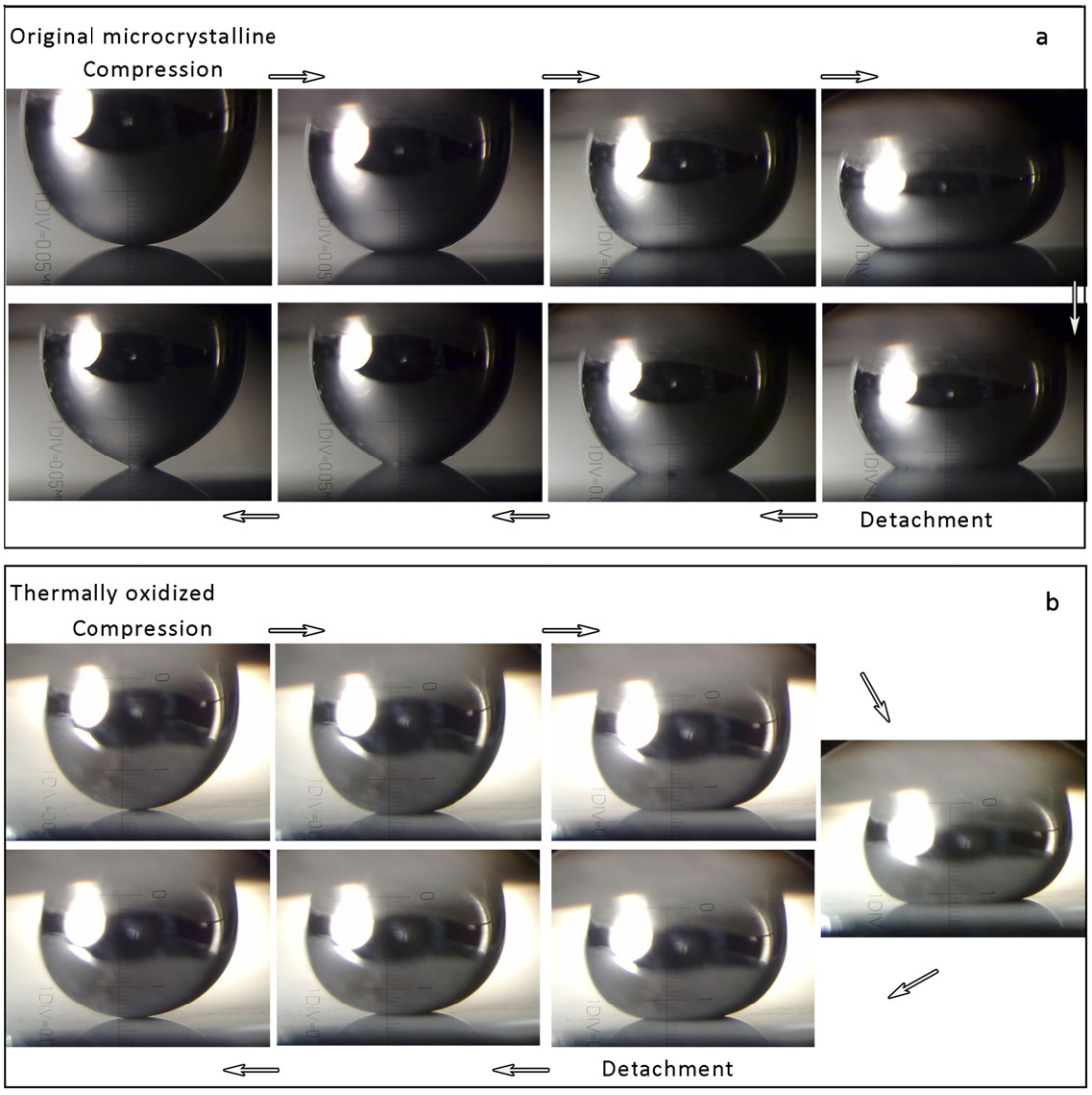

Fig. 8. Contact angle hysteresis with mercury. Progressive compression/detachment cycles (100 μm steps) of a mercury drop on the original microcrystalline surface (top) and on the oxidized one (bottom). Note that the contact angle hysteresis is practically zero on the oxidized surface, while the pronounced adhesion with the microcrystalline one leads to a large contact angle hysteresis. For these tests, mercury drops are adhered to the upper plate with double sided pressure sensitive adhesive tape.

The images on the lower row of Fig. 7 show the radical difference between the strength of the adhesion of mercury drops to the three surfaces. The pronounced deformation of the drop during its detachment from the polished single crystal (Fig. 7e) and from the microcrystalline surface (Fig. 7f) is absent when the drop detaches from the oxidized one (Fig. 7g). The contact angle for this later surface is practically 180°. This effect can be further appreciated in Fig. 8, which shows progressive compression/decompression cycles (100-μm steps) of a mercury drop on both the oxidized and on the microcrystalline surfaces.

The values of the corresponding contact angles are shown in Fig. 9. The contact angle hysteresis practically vanishes in the case of the oxidized surface, while the microcrystalline one presents a large CAH. Note also that the magnitude of the advancing contact angle starts off being very similar for both surfaces, but decreases more rapidly for the microcrystalline film due to the higher adhesion of this film.

4. Discusion

From the values of the contact angles and the information on the geometry of the pyramids we can infer which particular mechanism is responsible for the increased mercuryphobic and hydrophobic states we observe. Young's relation [4] is the starting point for calculating contact angles, θ_E, in a variety of circumstances, and is given by

$$\cos(\theta_E) = \frac{\gamma_{sv} - \gamma_{sl}}{\gamma_{lv}}, \quad (1)$$

where γ_{sv}, γ_{sl}, and γ_{lv} are the surface tensions at the solid–vapor, solid–liquid and liquid–vapor interface, respectively. Two particular wetting regimes are distinguished for rough surfaces. In the first one, it is energetically favorable for the system if the liquid conforms to the profile of the surface. In this case, (Wenzel's model [15]) the apparent contact angle θ^* will be given by

$$\cos(\theta^*) = r\cos(\theta_E), \quad (2)$$

where r is the surface roughness ratio, defined as the ratio between the actual surface area and the apparent surface area of the surface. The second regime may be entered as the surface roughness increases, at a point where the liquid detaches locally from the solid and traps air pockets at the valleys of the profile. In that case, we can think of the rough surface as a flat one but composed of two different chemical species, one of which is air (with contact angle equal

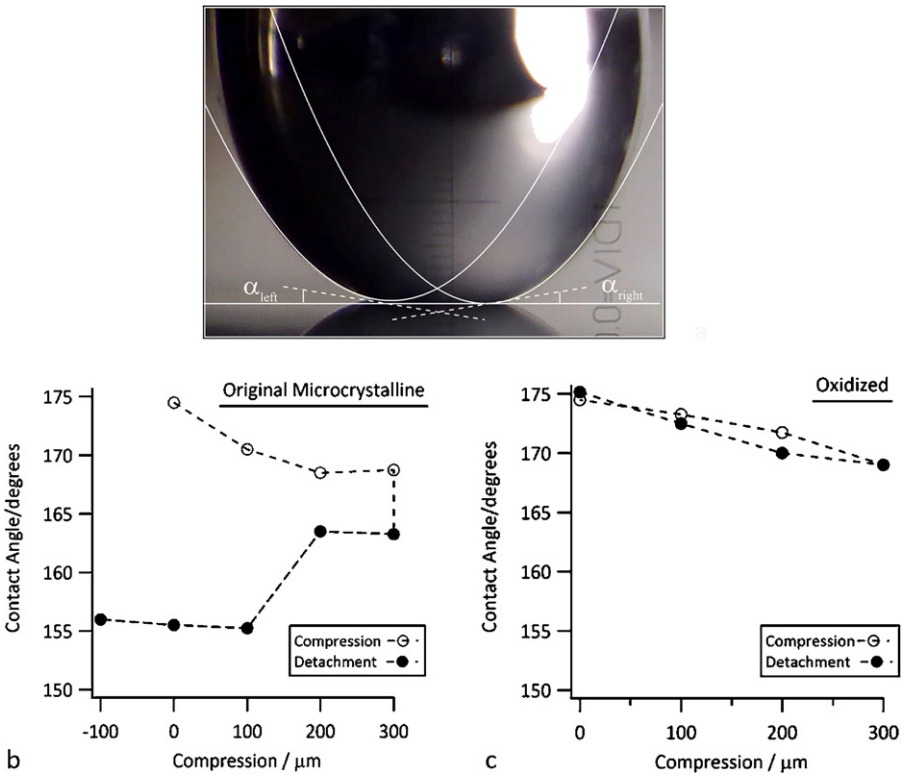

Fig. 9. Vanishment of the CAH with mercury. (a) Example of a contact angle measurement ($\theta^* = 180 - \alpha$) performed by approximating the profile of the drop close to the contact with a parabola. Due to image pixilation, the precision of the measurement was +- 0.5°. Average difference between left and right angles was 1°. (Lower graphs) Average contact angles (left + right/2) during the compression/detachment cycles (Fig. 8) of mercury drops on (b) the microcrystalline surface and (c) on the oxidized one. Note that contact angle hysteresis vanishes for the oxidized surface, while it is very pronounced for the original microcrystalline one.

to θ_E), and the other is the solid itself (with contact angle equal to θ_E). The characteristics of the surface's profile come in through the fractional surface area ϕ_s that is in contact with the liquid. This is the Cassie–Baxter [4,14] model and predicts an apparent contact angle θ^* given by the relation

$$\cos(\theta^*) = -1 + \phi_s(1 + \cos(\theta_E). \quad (3)$$

In both cases, Young's relation is assumed to hold locally. Energy minimization [4,37] dictates that air trapping will become possible when $\theta_E > \theta_c$, where

$$\cos(\theta_c) = -\frac{1 - \phi_s}{r - \phi_s}. \quad (4)$$

For conical pyramids with smooth walls and relatively small tops ($\phi_s \ll 1$), $\cos(\theta_c) \approx -\frac{1}{r}$ is equal to $\cos(\mu)$, where μ is the angle between the external surface of the walls and the horizontal axis as defined above. Then, the necessary condition to trap air at the interface becomes $\theta_E > \mu$. Since $\mu \sim 158°$ (section II.2) and $\theta_E = 155°$ for mercury and $\theta_E = 91°$ for water, Wenzel's model should in principle apply in both cases. But the fact that the contact angle between the oxidized surface and mercury is so close to 180° suggests that the protrusions on the surface (Fig. 2) may be playing a major role and actually be promoting the trapping of air pockets. If so, the mercury drop would be at the most in contact with the tops of the pyramids. This assumption can lead to a calculation of a lower limit of θ^* starting from the value of the contact angle with the polished surface ($\theta_E = 155°$) and the ratio of the typical area of the tops of the pyramids and the average size of the original microcrystals, or $\phi_s = (0.2 \times 0.2\ \mu m^2/10\ \mu m^2) = 4 \times 10^{-3}$. Plugging these values in equation (3) we obtain $\theta^* = 178.5°$ as the lower limit for the contact angle between the oxidized surface and mercury, which is in good agreement with the observed contact angle in Fig. 7g. Experiments on the hydrophobic enhancement of surfaces brought about the presence of two different texture scales [3,11,34] strongly suggest that it is precisely the protrusions that we measure on the tops of the pyramids what makes this possible. Furthermore, Cottin-Bizonne et al. [35] have shown that nano-patterned interfaces can induce a phase transition of the wetting state, depending on both the macroscopic parameters (pressure and contact angle) and the nanoscopic geometric details of the protrusions. They find that below a critical pressure, a low-friction composite phase is favored over a wetting one. Actually, robust super-hydrophobic surfaces induced by nano-scale protrusions have been fabricated using functionalized carbon nanotube forests [36]. Regarding the apparent complete reversibility of the compression process of the mercury drops on this surface, Lapierre et al. [37,38] have found that multiple specific length-scales are also necessary to achieve robust reversibility of the CA in electrowetting experiments. Thus, we believe that the protrusions shown in Fig. 2 are responsible for the super-mercuryphobic state we observe.

For water on the original microcrystalline sample, the relatively small increase in contact angle compared to the polished single crystal surface indicates that the system is in Wenzel's regime. In the case of the contact with both the oxidized and the nano-patterned surfaces, it is possible that we have reached the metastable part of the air trapping regime. Indeed we find that upon removal of a water drop with a micropipette, a drop of water with very low contact angle (<30°) is left on both surfaces. This transition from a hydrophobic to a hydrophilic state is typical of systems that are on a metastable Cassie wetting state [9,17].

We note that the increased hydrophobicity of the nano-patterned surface is due partially to the increased roughness of

the film, and partially to the natural hydrophobicity of the silane compound. The fact that the polished surface is barely hydrophobic ($\theta_E = 91^\circ$) makes it very hard for any roughening of the surface to significantly change the wetting properties on its own [4]. A much higher density of nano-globules would be needed to achieve this goal.

The impressive vanishment of the CAH we find for the oxidized surface in contact with mercury is consistent with the fact that drops of this liquid roll out of the surface at an apparent zero tilt-angle [39]. This reversibility implies that mercury drops do not wet the oxidized surface. Furthermore, given the smooth dependence of the CA on the compression (Fig. 9b), we can assert that this Cassie state is robust [36]. We note that the correct thermodynamic variable needed to make this assertion is the pressure and not the compression. Therefore, either measuring directly the reaction force or calculating the pressure from the profile of the deformed drop, would be necessary to properly quantify the limit of this robustness.

On the other hand, the large CAH measured between the original microcrystalline sample and the mercury drop indicates that there are portions of the surface that pin the contact line during detachment [4]. A large CAH is usually observed on surfaces that are not rough enough to enter the stable portion of Cassie's regime [13]. The sharp edges of the micron sized crystals are probably playing the role of such pinning points. It would be interesting to study the dynamics of the contact line for this surface.

5. Conclusions

Progressive roughening of diamond surfaces leads to increasingly higher contact angles with water drops up to 138°, while for mercury drops a super-mercuryphobic state is observed ($CA > 175^\circ$).

Thermal oxidation of a microcrystalline diamond surface creates pyramids with sub-micron protrusions that increase both the hydrophobic and mercuryphobic properties of the film. For water, a metastable Cassie state is reached, while for mercury, this surface is non-wettable for this liquid (robust Cassie wetting state).

The contact angle hysteresis vanishes for the contact between mercury drops and the oxidized surface in compression/detachment cycles, for which the maximum compression is of the same order of magnitude as the size of the drops. This vanishment of the CAH is consistent with the fact that mercury drops roll along out of the surface at an apparent zero tilt-angle [39]. The impressive low adhesion we observe resembles that of liquid drops covered with hydrophobic powders, or "liquid marbles" [40]. In this respect, it would be very interesting to measure the small adhesion involved in this system. Since measuring the contact angle become increasingly hard as the CA approaches 180° (in particular due to the high mobility of the drops [41]), measuring the force of adhesion directly with a force microscope [42] would be more adequate. This work is underway.

Finally, for the contact with water, silanization of the oxidized surface creates nano-globules of 35 nm in diameter that increase the hydrophobic properties of the film up to a contact angle of 138°. This is a rather modest value compared to the high contact angles ($\sim 170^\circ$) that are achievable with nano-tube coatings [43] or with "nano-grass" on boron doped diamond [19] ($CA \sim 160^\circ$). A higher density of nano-globules than the one obtained in this work might make the oxidized diamond surface super-hydrophobic. In future work, it would be interesting to measure the effects of the deposition of monolayers of PTA or PFTS on the hydrophobicity of our oxidized sample, given the good results these coating have yielded on other boron-doped diamond systems [19].

Acknowledgements

JVE gratefully acknowledges financial support from DGAPA's postdoctoral fellowship CJIC/CTIC/2135/2009 and CONACYT'S graduate division postdoctoral fellowship (CVU 37905). We acknowledge financial support from DGAPA-UNAM funds (IN-104911). We also thank Jorge Barreto, Carlos Magaña, Mario Monroy, and Lázaro Huerta for assistance at different stages of the characterization and instrumentation. We thank Arturo Menchaca-Rocha for useful discussions, Anna Kozina for assistance during the silanization process and Seth Putterman for lending us the doped single crystalline diamond.

References

[1] B. Bhushan, Langmuir 28 (2012) 16982.
[2] Z.G. Guo, W.M. Liu, B.L. Su, Journal of Colloid and Interface Science 353 (2011) 335.
[3] D. Bonn, J. Eggers, J. Indekeu, J. Meunier, E. Rolley, Reviews of Modern Physics 81 (2009) 739.
[4] P.G. De Gennes, F. Brochard-Wyart, D. Quere, Capillarity and Wetting Phenomenae, Springer, USA, 2002.
[5] A.J. Walton, Advances in Physics 26 (1977) 887.
[6] S. Herminghaus, M. Brinkmann, R. Seemann, Annual Reviews of Materials Research 38 (2008) 101.
[7] A. Marmur, Soft Matter 8 (2012) 2867.
[8] M. Nosonovsky, B. Bhushan, Journal of Adhesion Science and Technology 22 (2008).
[9] N. Verplanck, Y. Coffinier, V. Thomy, R. Boukherroub, Nanoscale Research Letters 2 (2007) 577.
[10] S. Shibuichi, T. Onda, N. Satoh, K. Tsujii, Journal of Physical Chemistry 100 (1996) 19512.
[11] M. Noscinovsky, B. Bhushan, Langmuir 24 (2008) 1525.
[12] A. Menchaca-Rocha, Journal of Colloid and Interface Science (1992) 472.
[13] R.E. Johnson, R.H. Dettre, Contact angle hysteresis, in: Contact Angle, Wettability and Adhesion, ACS Advances in Chemistry Series, vol. 43, American Chemical Society, Washington, DC, 1964, pp. 112–135.
[14] A.B.D. Cassie, S. Baxter, Transactions of Faraday Society 40 (1944) 546–551.
[15] R.N. Wenzel, Industrial and Engineering Chemistry 28 (1936) 988.
[16] J.F. Joanny, P.G. De Gennes, Journal of Chemical Physics 81 (1984) 552.
[17] A. Lafuma, D. Quere, Nature Materials 2 (2003) 457.
[18] M. Wang, N. Simon, C. Decorse-Pascanut, M. Bouttemy, A. Etcheberry, M.S. Li, R. Boukherroub, S. Szunerits, Electrochimica Acta 54 (2009) 5818.
[19] Y. Coffinier, E. Galopin, S. Szunerits, R. Boukherroub, Journal of Materials Chemistry 20 (2010) 10671.
[20] L. Marcon, A. Addad, Y. Coffinier, R. Boukherroub, Acta Biomaterialia 9 (2013) 4585.
[21] H. Linke, B.J., Aleman, L.D., Melling, M.J., Taormina, M.J., Francis, C.C. Dow-Hygelund, V., Narayanan, R.P., Taylor, A., Stout, Physical Review Letters 96 (2006).
[22] US Department of Health and Human Services (DHHS): NIOSH Pocket Guide to Chemical Hazards, National Institute for Occupational Safety and Health (NIOSH), Publication No. 2005-149 (2007, September).
[23] P. John, N. Polwart, C.E. Troupe, J.I.B. Wilson, Diamond and Related Materials 11 (2002) 861.
[24] S. Ghodbane, T. Haensel, Y. Coffinier, S. Szunerits, D. Steinmuller-Nethl, R. Boukherroub, S.I.U. Ahmed, J.A. Schaefer, Langmuir 26 (2010) 18798.
[25] M. Wang, N. Simon, G. Charrier, M. Bouttemy, A. Etcheberry, M.S. Li, R. Boukherroub, S. Szunerits, Electrochemistry Communications 12 (2010) 351.
[26] J. Ristein, Surface Science 600 (2006) 3677.
[27] X.F. Wang, A.R. Ruslinda, Y. Ishiyama, Y. Ishii, H. Kawarada, Diamond and Related Materials 20 (2011) 1319.
[28] F. Klauser, S. Ghodbane, R. Boukherroub, S. Szunerits, D. Steinmuller-Nethl, E. Bertel, N. Memmel, Diamond and Related Materials 19 (2010) 474.
[29] S. Kaciulis, Surface and Interface Analysis 44 (2012) 1155.
[30] S.T. Jackson, R.G. Nuzzo, Applied Surface Science 90 (1995) 195.
[31] D. Ballutaud, T. Kociniewski, J. Vigneron, N. Simon, H. Girard, Diamond and Related Materials 17 (2008) 1127.
[32] L. Ostrovskaya, V. Perevertailo, V. Ralchenko, A. Dementjev, O. Loginova, Diamond and Related Materials 11 (2002) 845.
[33] M. Karlsson, P. Forsberg, F. Nikolajeff, Langmuir 26 (2010) 889.
[34] X.C. Li, B.K. Tay, P. Miele, A. Brioude, D. Cornu, Applied Surface Science 255 (2009) 7147.
[35] C. Cottin-Bizonne, J.L. Barrat, L. Bocquet, E. Charlaix, Nature Materials 2 (2003) 237.
[36] C. Journet, S. Moulinet, C. Ybert, S.T. Purcell, L. Bocquet, Europhysics Letters 71 (2005) 104.

[37] F. Lapierre, V. Thomy, Y. Coffinier, R. Blossey, R. Boukherroub, Langmuir 25 (2009) 6551.
[38] F. Lapierre, P. Brunet, Y. Coffinier, V. Thomy, R. Blossey, R. Boukherroub, Faraday Discussions 146 (2010) 125.
[39] E.B. Dussan, R.T.P. Chow, Journal of Fluid Mechanics 137 (1983) 1.
[40] S. Moulinet, D. Quere, Nature 411 (2001) 924.
[41] M. Callies, D. Quere, Soft Matter 1 (2005) 55.
[42] R. Budakian, S.J. Putterman, Applied Physics Letters 81 (2002) 2100.
[43] K.K.S. Lau, J. Bico, K.B.K. Teo, M. Chhowalla, G.A.J. Amaratunga, W.I. Milne, G.H. McKinley, K.K. Gleason, Nano Letters 3 (2003) 1701.